High-Efficiency Grating Coupler in 400 nm and 500 nm PECVD Silicon Nitride With Bottom Reflector

Volume 11, Number 5, October 2019

Siddharth Nambiar, *Member, IEEE*
Abhai Kumar
Rakshitha Kallega
Praveen Ranganath
Shankar Kumar Selvaraja, *Senior Member, IEEE*

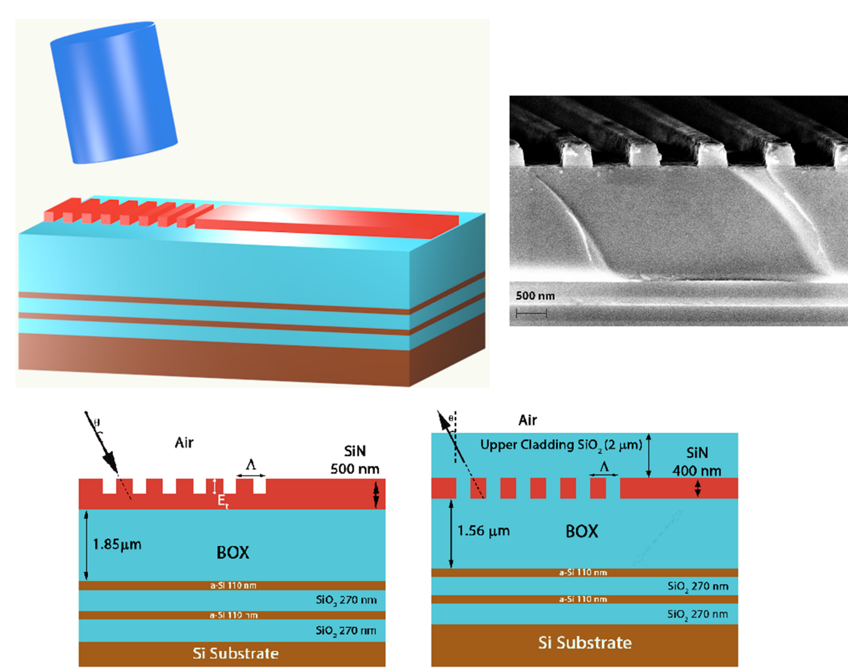

DOI: 10.1109/JPHOT.2019.2936430

High-Efficiency Grating Coupler in 400 nm and 500 nm PECVD Silicon Nitride With Bottom Reflector

Siddharth Nambiar[1] ***Member, IEEE*****, Abhai Kumar**[1,2]
Rakshitha Kallega[1] **Praveen Ranganath**[1]
and Shankar Kumar Selvaraja[1] ***Senior Member, IEEE***

[1]Centre for Nano Science and Engineering (CeNSE), Indian Institute of Science (IISc), Bangalore 560012, India
[2]Defence Materials and Stores Research and Development Establishment-DRDO Labs, Kanpur 208013, India

DOI:10.1109/JPHOT.2019.2936430
This work is licensed under a Creative Commons Attribution 4.0 License. For more information, see https://creativecommons.org/licenses/by/4.0/

Manuscript received June 3, 2019; revised August 4, 2019; accepted August 14, 2019. Date of publication August 21, 2019; date of current version September 6, 2019. This work was supported in part by the DST-SERB and in part by the Ministry of Human Resource Development (MHRD) through NIEIN Project, from MeitY and Department of Science and Technology (DST) through Nanoelectronics Network For Research and Application (NNetRA). Corresponding author: Siddharth Nambiar (e-mail: sidnam12@gmail.com).

Abstract: We design and experimentally demonstrate highly efficient Silicon Nitride based grating couplers with bottom distributed Bragg reflectors. All the layers were deposited using plasma enhanced chemical vapor deposition processing. We present gratings on two Silicon Nitride thickness (400 nm and 500 nm) platforms. On a 500 nm thick Silicon Nitride, we show a peak coupling efficiency of −2.29 dB/coupler at a wavelength of 1573 nm with a 1 dB bandwidth of 49 nm. On a 400 nm thick platform, we demonstrate a coupling efficiency of −2.58 dB/coupler at 1576 nm with a 1 dB bandwidth of 52 nm. The demonstrated coupling efficiency is the best reported as yet, for both 400 nm and 500 nm thick, plasma deposited Silicon Nitride platforms.

Index Terms: Grating couplers, silicon nitride, waveguides.

1. Introduction

Silicon Nitride (SiN) is emerging as an alternative CMOS compatible material platform for on-chip linear and non-linear applications. Unlike Silicon, SiN is transparent in visible to mid-infrared wavelength range, making it attractive for applications ranging from bio to molecular sensing [1], [2]. Recent demonstration of various essential functional building blocks in SiN [3]–[5] clearly show the migration towards SiN as a platform for many applications. In addition to transparancy, SiN offers various advantages, including low-loss, less sensitivity to temperature and fabrication variation, and CMOS fabrication technology compatibility. As opposed to Silicon, SiN does not exhibit two photon absorption in the near-infrared regime and so SiN is an ideal candidate for numerous nonlinear optical applications [6]–[8]. The ability to tune the thickness and refractive index offers additional flexibility in engineering dispersion for a broad range of wavelengths.

In photonic integrated circuits, efficient coupling of light between fiber and chip is essential to realize desired on-chip functionality. Surface grating couplers are a preferred means of coupling as they offer compatibility with wafer-level testing and are alignment tolerant. Optical quality SiN films

are deposited either using low pressure chemical vapor deposition (LPCVD) or plasma enhanced chemical vapor deposition (PECVD) at high and low process temperatures respectively. Most of the fiber-to-chip grating coupler demonstrations in literature were demonstrated on LPCVD SiN [9]–[14]. Though stoichiometric SiN deposited through LPCVD process offers better material quality, the film thickness is limited due to high stress [15], [16]. To overcome this stress limitation, several approaches have been suggested such as engineering deep trenches to form a crack free region [17], thermal cycling [18], pre-patterning substrates using photonic damascene process [19], as well as pilfering stoichiometry by depositing Silicon-rich nitride [20], [21]. All of the aforementioned approaches entail deposition temperatures, usually in excess of 750 °C and therefore demand a higher thermal budget. Furthermore, a high process temperature restricts the substrate type, such as, metal or dielectric reflectors [22]. PECVD based processes on the other hand offer a low cost, low temperature ($<$400 °C) alternative that is back end of line (BEOL) CMOS compatible [23]. Consequently there has been a renewed interest towards developing a low temperature SiN platform for linear [24] as well as nonlinear photonics [25]–[28]. One of the drawbacks of using PECVD process is the material absorption loss due to N-H bond, which is typically addressed using high temperature annealing ($>$1000 °C) [29]. On the other hand, it has been reported that lower propagation loss of up to -1.5 dB/cm [30] is achievable in C-band by reducing the hydrogen content, employing only N_2 and SiH_4 as deposition precursors and up to -1 dB/cm in C-L band spectrum by using the same approach in an inductively coupled plasma-CVD [31]. Despite their low-loss potential, there have been few reported works on grating couplers using standalone PECVD SiN platforms in the O-L band region, among which the best so far has been -2.56 dB/coupler, demonstrated on a 220 nm thick SiN platform [32]. In this work, we present high-efficiency gratings for Transverse Electric (TE) mode coupling in standalone 500 nm and 400 nm thick PECVD SiN platforms, which is an extended account of preliminary results reported in [33].

The coupling efficiency of a surface grating coupler depends primarily on two factors, which is directionality and fiber-to-grating mode matching. Directionality is the proportion of total power scattered towards the coupling fiber. Since the grating phase matching allows for equal coupling to both top and bottom regions, it is essential that the power leaked to the latter is recycled back to the waveguiding layer. This can be achieved by inserting a bottom reflector at an optimum buried oxide (BOX) thickness which allows for constructive interference of the reflected light with the original upward scattered light. On crystalline SOI, incorporating a bottom reflector can be cumbersome as it involves complex processing steps like flip-chip [34] or plasma bonding [35] to a carrier wafer or a backside metallization [36]. On SiN however, a distributed Bragg reflector (DBR) stack and the waveguiding layers can be deposited in a sequential manner [11]. Moreover, grating couplers with amorphous Silicon (a-Si) and SiO_2 as DBR stack have already been demonstrated on deposited SOI with a high coupling efficiency of -1.6 dB/coupler [37].

2. Design and Simulation

The grating couplers were designed and optimized using FDTD solver from Lumerical. The couplers were designed using the basic Bragg condition where a first-order diffraction grating period can be expressed as,

$$\Lambda = \frac{\lambda}{n_{eff} - n_c \sin\theta} \tag{1}$$

where n_{eff} is the effective grating index, n_c is the top cladding index which in this case is that of air and θ is the fiber inclination angle. Accordingly, n_{eff} is calculated as:

$$n_{eff} = d_c n_{etch}^{TE_{00}} + (1 - d_c) n_{SiN}^{TE_{00}} \tag{2}$$

where d_c is the duty cycle, $n_{SiN}^{TE_{00}}$ and $n_{etch}^{TE_{00}}$ are the effective indices of the fundamental TE_{00} mode for the SiN slab and etched regions respectively. The refractive indices of c-Si (crystalline Silicon), a-Si, SiO_2, and PECVD SiN are obtained from ellipsometry to be 3.46, 3.53, 1.44 and 2.015 respectively. Fig. 1(a) illustrates various power distribution channels in a generic grating. For simulation and

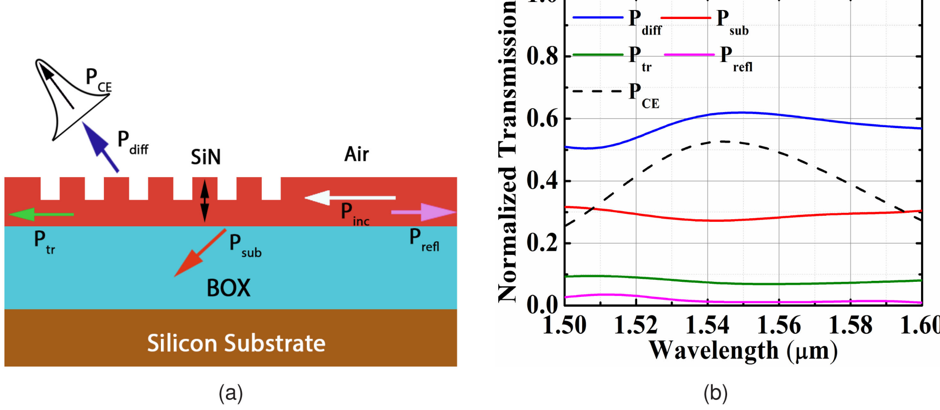

(a) (b)

Fig. 1. (a) 2D schematic of a grating coupler used in simulations along with a depiction of different power loss channels. (b) Simulated spectral characteristics of an optimized grating and its coupling performance with a 1.05 μm period, 55% duty cycle, 9.5° incident angle and 270 nm etch depth.

optimisation, a TE polarized Gaussian beam, with mode field diameter of 10.4 μm, is used as a source which is embedded in the air region. The coupling efficiency is estimated by monitoring the power coupled to the fundamental mode in the SiN slab layer. The incident power P_{inc} and power coupling to fiber P_{CE} is expressed as,

$$P_{\text{inc}} = P_{\text{diff}} + P_{\text{sub}} + P_{\text{refl}} + P_{\text{tr}} \tag{3}$$

$$P_{\text{CE}} = \eta P_{\text{diff}} \tag{4}$$

where P_{diff} represents the directionality or power diffracted to the air region, P_{sub} the substrate leakage, P_{refl} denotes the back reflection and P_{tr} signifies the power transmitted through the grating. η expressed as $\int_S |E_g \times H_f^* dS|^2$, is the mode field overlap [38] between the diffracted grating field (E_g) and the Gaussian fiber mode field (H_f). It is clear that both η and P_{diff} need to be maximized to achieve high coupling performance. In the following sections, we present grating coupler design and simulation summary for 500 nm and 400 nm thick SiN. A parametric sweep of the grating period, duty cycle, etch depth, BOX thickness and source inclination angles is done to achieve maximum power coupling P_{CE}.

2.1 Gratings on 500 nm SiN

The spectral response of the optimized grating for the 500 nm thick SiN/air design and its coupling efficiency (CE) is depicted in Fig. 1(b). A peak CE of 52.5% is achieved at 1.544 μm for a period Λ of 1.05 μm, duty cycle d_c of 55%, etch depth E_t of 270 nm, inclination angle θ of 9.5° and a BOX thickness of 1.9 μm. While P_{diff} is observed to be 55–60% in most part of the spectrum, the substrate leakage P_{sub} accounts for a substantial portion of the total scattered power loss (~30%). The remaining losses, P_{tr} and P_{refl}, together contribute a little under 10% of the total loss. In order to curtail P_{sub} and enhance directionality, we incorporate a bottom reflector using two layer DBR stack consisting of sequential layers of 110 nm and 270 nm thick a-Si and SiO_2 respectively. A schematic of the grating device with bottom reflector used in simulations is shown in Fig. 2(a). The thickness of the oxide layer between the grating and the bottom reflector is crucial to achieve phase matching between the bottom reflected field and the scattered field from the grating. Fig. 2(b) plots the variation of peak CE as a function of BOX thickness for the optimized grating period, with and without a DBR stack. The plot indicates a slightly lower optimal BOX thickness for a DBR stack at 1.85 μm, when compared to a Si substrate. The peak efficiency is observed to be over 70% within a ±50 nm deviation of optimal BOX thickness. We observe an optimal simulated coupling efficiency

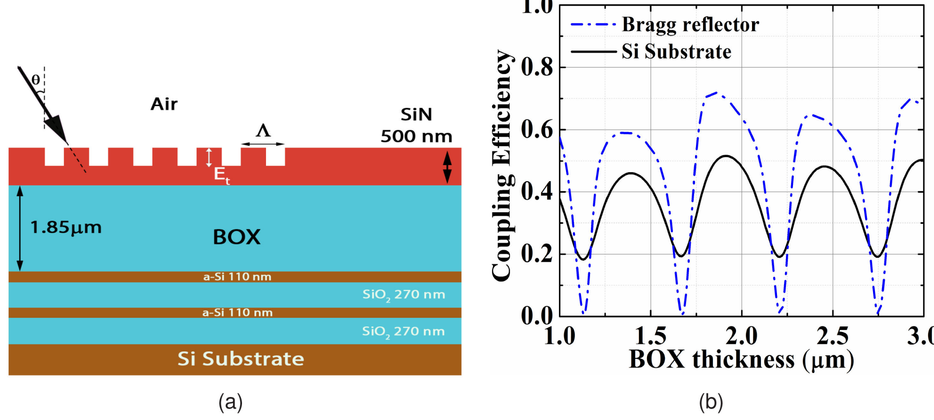

Fig. 2. (a) 2D schematic of a grating coupler with a bottom DBR stack. (b) Effect of BOX thickness on the coupling efficiency at 1.55 μm of an optimized grating with and without a DBR stack.

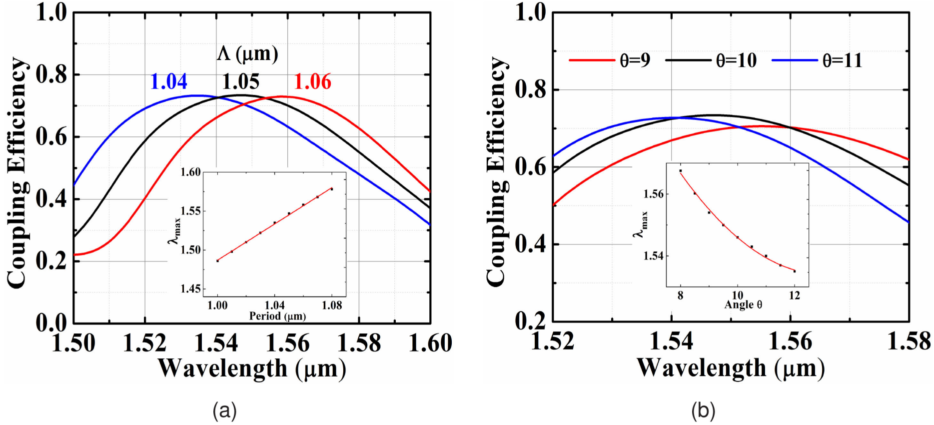

Fig. 3. Effect of grating (a) period Λ and (b) fiber inclination angle θ on the spectral characteristics and coupling efficiency of the grating coupler in 500 nm thick SiN. Inset in both graphs show the peak wavelength evolution. For (b), a grating period of 1.05 μm, duty cycle 55% and etch depth 260 nm is used to simulate the effect of inclination angle.

of 73.4% at a wavelength of 1.547 μm with a 1 dB bandwidth of 56 nm. The coupling is 20% higher than the design without DBR. Maximum coupling is observed for a period of 1.05 μm, which is same as that of grating without DBR, at 10° inclination angle and an etch depth of 260 nm. Fig. 3 shows the CE variation as a function of grating period and inclination angle. The peak coupling wavelength λ_{max} increases linearly with Λ while an inverse relation with θ is observed which is consistent with eq. (1). The dependence of d_c at optimized period is depicted in Fig. 4(a). While maximum coupling is observed for 55% d_c, the peak efficiency is maintained above 72% for a 5% variation in d_c. Fig. 4(b) depicts the variation of peak CE at different etch depths. We estimate a 1 nm decrease in λ_{max} per nm increase in etch depth E_t. For an etch span of 80 nm, the peak coupling is observed to be over 70%, with a noticeable red shift in λ_{max} at lower E_t, which underlines the robustness of design to process induced etch variations.

2.2 Gratings on 400 nm SiN

Using eqs. (1) and (2) and employing a similar methodology as described for 500 nm thick SiN/air grating design, we optimize the grating coupler parameters for a 400 nm thick SiN in SiO_2 cladding

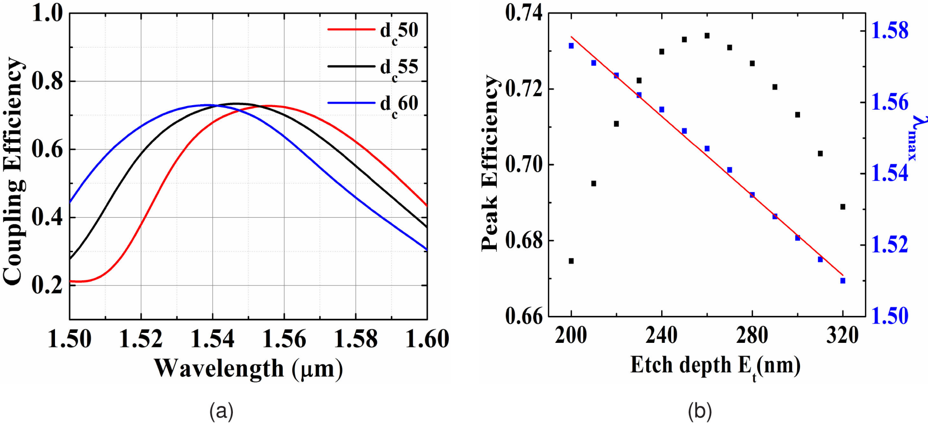

Fig. 4. Effect of (a) duty cycles and (b) etch depth on the efficiency of grating coupler in 500 nm thick *SiN*. In (b), coupling efficiency variation as well as peak wavelength shift as function of etch depth is presented for 1.05 μm period and 10° inclination angle.

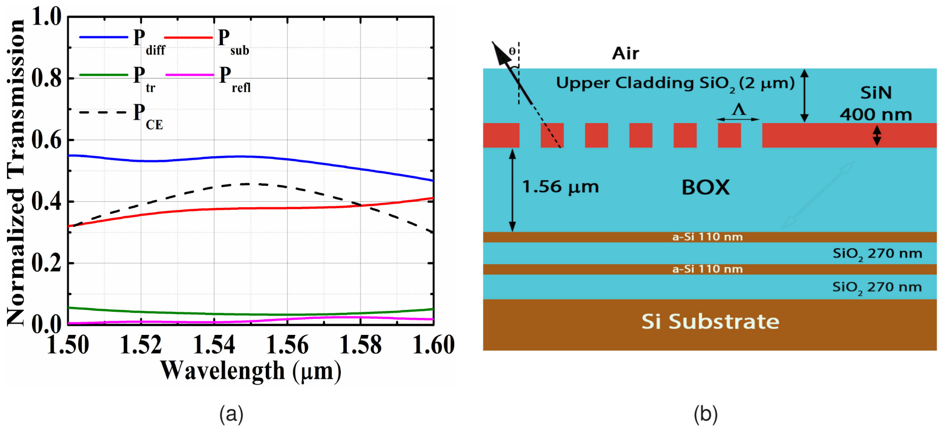

Fig. 5. (a) Optimized grating spectrum with various loss channels for a 400 nm thick *SiN* grating coupler with *Si* substrate. (b) 2D schematic of a fully etched 400 nm thick *SiN* grating coupler with an underneath DBR mirror stack, similar to the one illustrated in Fig. 2(a).

to achieve maximum coupling efficiency between a Gaussian fiber source and the fundamental propagating mode. Unlike the previous case however, gratings in this design are considered as fully etched. Initially, the coupling is optimized for a *Si* substrate without a bottom reflector. The optimum BOX thickness is calculated to be 1.6 μm.

Fig. 5(a) shows the grating spectrum with the different loss channels for the optimized grating period. Peak coupling is observed to be 46.4% at a wavelength of 1.55 μm for an optimized grating with a period of 1.12 μm, 10° inclination angle, and 50% d_c. As also observed in the 500 nm device, principal loss is due to substrate leakage P_{sub}, which is above 35% in this case. The substrate leakage is reduced by adding a bottom DBR, similar to the one described in Section 2.1. A 2D schematic of the device design layout is illustrated in Fig. 5(b). Fig. 6(a) shows the coupling at different periods. With an underneath DBR, we observe a peak coupling efficiency of 77% which is an increase of about 30% at 1.575 μm with a 1 dB bandwidth of 75 nm. The peak coupling as a function of BOX thickness is plotted in Fig. 6(b). Here too, the optimal BOX thickness for a DBR stack is observed to be slightly lower at 1.56 μm which is similar to trend observed in the previous design. Also, a $\pm$50 nm variation in ideal BOX thickness leads to a marginal reduction

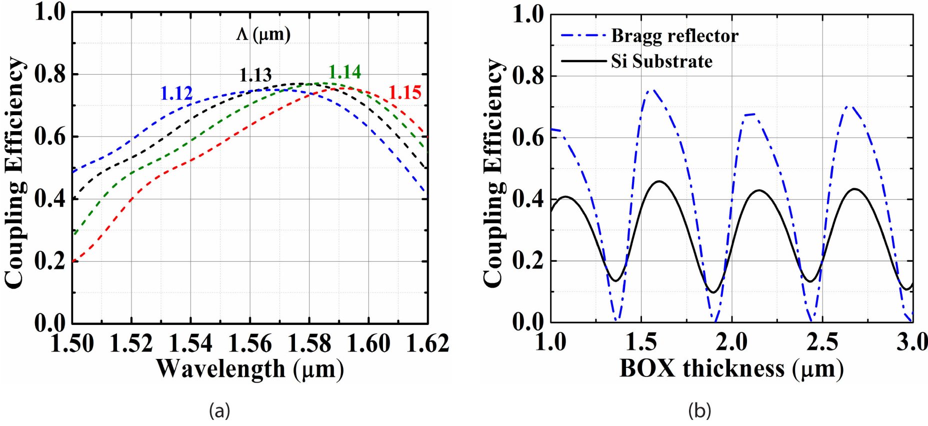

Fig. 6. (a) shows simulated coupling efficiency as function of period at 10° angle for gratings with DBR. A 50% duty cycle and 10° inclination angle was used for both simulations. (b) shows effect of BOX thickness on the coupling efficiency of an optimized grating in 400 nm thick SiN at 1.55 μm with and without a DBR stack.

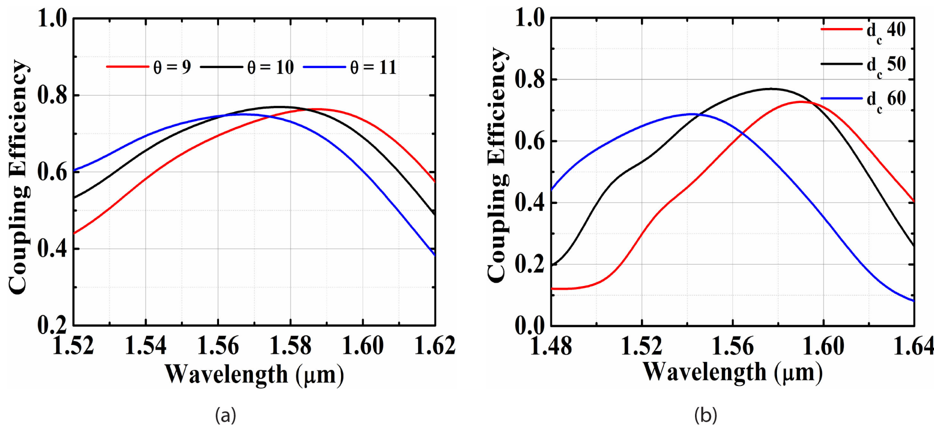

Fig. 7. Effect of (a) inclination angle θ and (b) duty cycles on spectral characteristics of an optimized grating with period of 1.13 μm in 400 nm thick SiN.

in coupling to 70%. Fig. 7(a) and 7(b) show the inclination angle and duty cycle dependence at optimum period. Maximum coupling efficiency is achieved with a grating period of 1.13 μm, 50% d_c, and 10° inclination. The grating being fully etched, offers a reliable platform that avoids etch depth variation.

2.3 Impact of DBR Stacks

Figure 8 showcases the dependence of coupling performance of the two optimized designs to the number of DBR stacks. For a single layer a-Si/SiO_2 stack, the calculated peak coupling is observed to be 68% for 500 nm SiN/air grating and 69% for 400 nm SiN/SiO_2 grating. However, for a 2 layer DBR stack, the corresponding peak coupling is observed to be 73% in the case of former and 77% in the case of latter. Beyond 2 layers, there is appears to be a saturation and no noticeable improvement in peak coupling performance of both designs. These plots indicate that a 2 level DBR stack underneath the BOX, would be sufficient to implement a highly directional grating design.

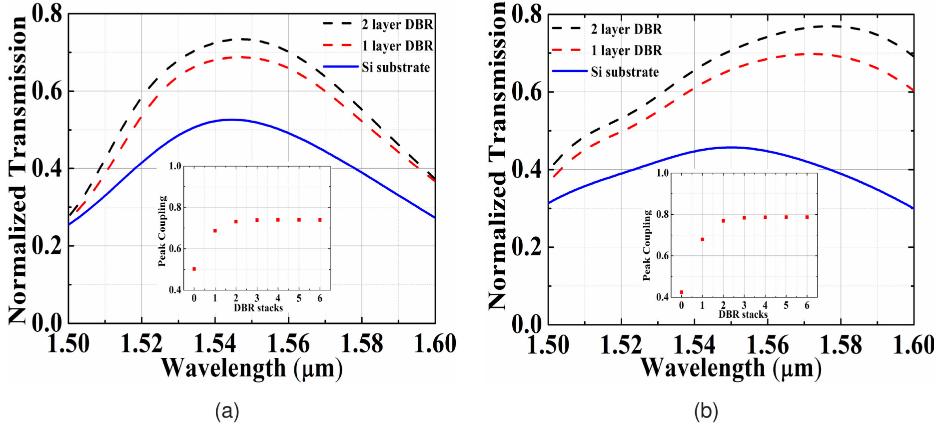

Fig. 8. Comparison of coupling spectrum between a grating with BOX over Si substrate and a 1 and 2 layer DBR stack for (a) 500 nm SiN/air gratings and (b) 400 nm SiN/SiO_2 gratings. In each case, the BOX thickness is fixed at the optimal value. Inset in each plot shows variation of peak coupling as a function of number of DBR stacks. 0 DBR implies a bare Si substrate.

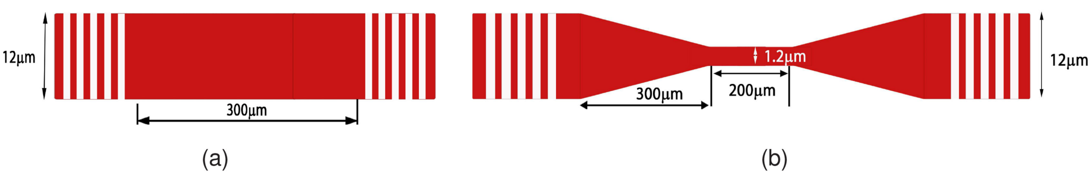

Fig. 9. Schematic of (a) patch waveguide gratings fabricated in 500 and 400 nm thick SiN platforms and (b) Rib waveguides with an adiabatic linear tapers fabricated on 500 nm SiN.

3. Fabrication and Characterization

The devices were fabricated on a *Si* wafer and all the material deposition was done using PECVD. Initially on a clean *c-Si* wafer, successive deposition of 270 nm SiO_2 and 110 nm of *a-Si* is done to create a bottom DBR. The layers are deposited twice to form a 2-layer DBR stack. The wafer with DBR stack is used a base substrate to build grating device demonstrator on 500 nm and 400 nm thick SiN. For the 500 nm thick SiN design, a 1.85 μm thick BOX layer is deposited followed by a 500 nm thick SiN using silane (SiH_4), ammonia (NH_3), and nitrogen (N_2) at 350 °C. For the 400 nm SiN device layer, 1.56 μm thick SiO_2 is used as BOX. The wafers with the SiN device layer and DBR, are used to pattern grating test structures. The fabricated test structures consisted of, a 12 μm wide and 300 μm long patch waveguide (as illustrated in Fig. 9(a)) for the 500 and 400 nm SiN platforms. In addition, a 200 μm rib waveguide with in and out 300 μm long adiabatic waveguide tapers (as shown in Fig. 9(b)) was fabricated on the 500 nm thick SiN platform.

The grating test structures were fabricated using Electron Beam Lithography (EBL) and dry etch process. The grating test patterns were written on MaN 2403 resist using EBL, followed by dry etching of SiN. The 400 nm devices were fully etched, while 500 nm thick SiN devices were partially etched to 260 nm. Grating periods and duty cycles were varied to study their effect on the device characteristics. The patterns in the resist were transferred into SiN using Fluorine chemistry with inductively coupled plasma-reactive ion etching (ICP-RIE) process. The remaining resist is removed using plasma resist strip and wet clean. As per the design, 400 nm devices were covered with 2 μm SiO_2. The process flow of the device stack for both designs is illustrated in Fig. 10. A scanning electron microscope (SEM) image of the fabricated devices is depicted in Fig. 11. Fig. 11(b),(d) shows the cross-section SEM of fabricated gratings of both platforms with their 2-layer bottom DBR stack.

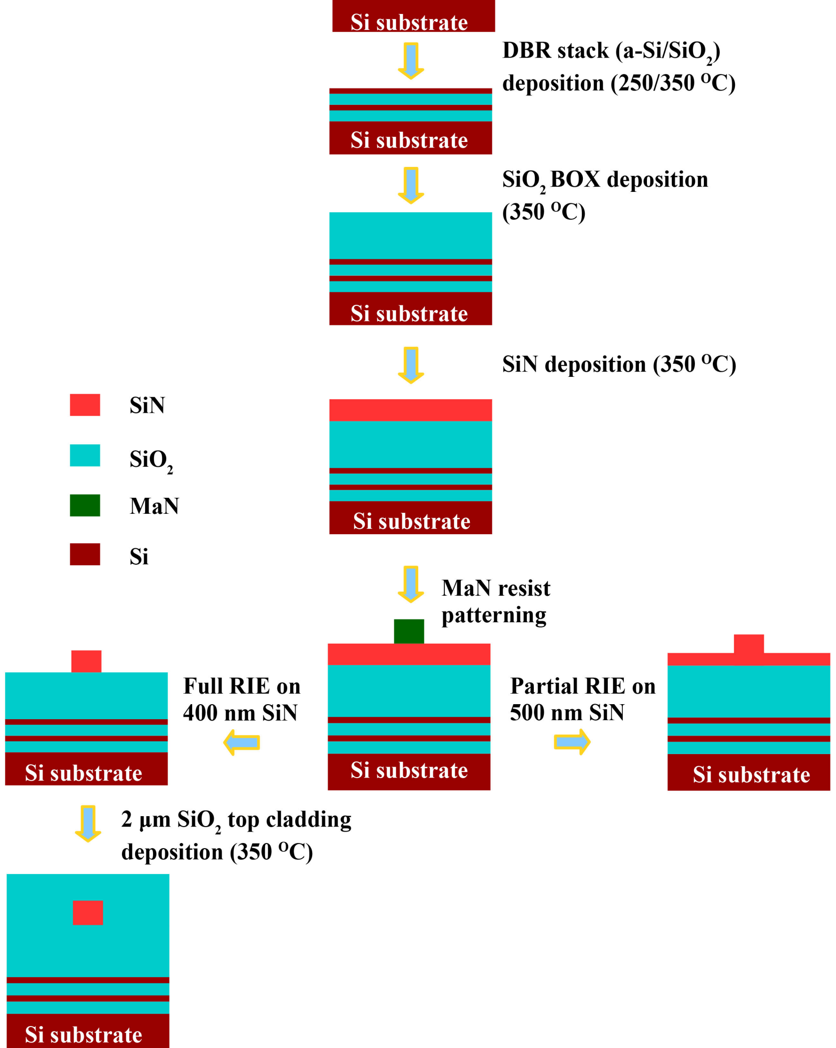

Fig. 10. Fabrication process flowchart for grating couplers on 500 nm and 400 nm *SiN*. All depositions were done on a standard PECVD chamber and the deposition temperatures did not exceed 350 °C.

Optical characterization was done using a fiber coupler C-band, superluminescent laser diode (SLD) as a light source and an optical spectrum analyser (OSA). The in and out coupling fibers are mounted on a gonio stage to characterize the effect of incident angle on the device performance. Light from SLD is coupled to in-coupling fiber through a polarization controller. The output port fiber from the stage is connected to an OSA. The efficiency of the device is calculated by normalizing the device spectra from the source spectra without the device.

4. Results and Discussion

Figure 12 shows a summary of coupling efficiencies of grating couplers fabricated on 500 nm thick *SiN*/air platform. A maximum coupling efficiency of −2.29 dB per coupler was measured at 1573 nm with a 1 dB bandwidth of 49 nm. The maximum efficiency was achieved with a period of 1.04 μm, 55% duty-cycle and 8.5° fiber inclination angle. With increasing grating period, we observe a red-shift of the peak wavelength, however, with only marginal change (±0.1 dB) in the coupling efficiency as shown in Fig. 12(a). We observe a wavelength shift of 0.8 nm/nm in

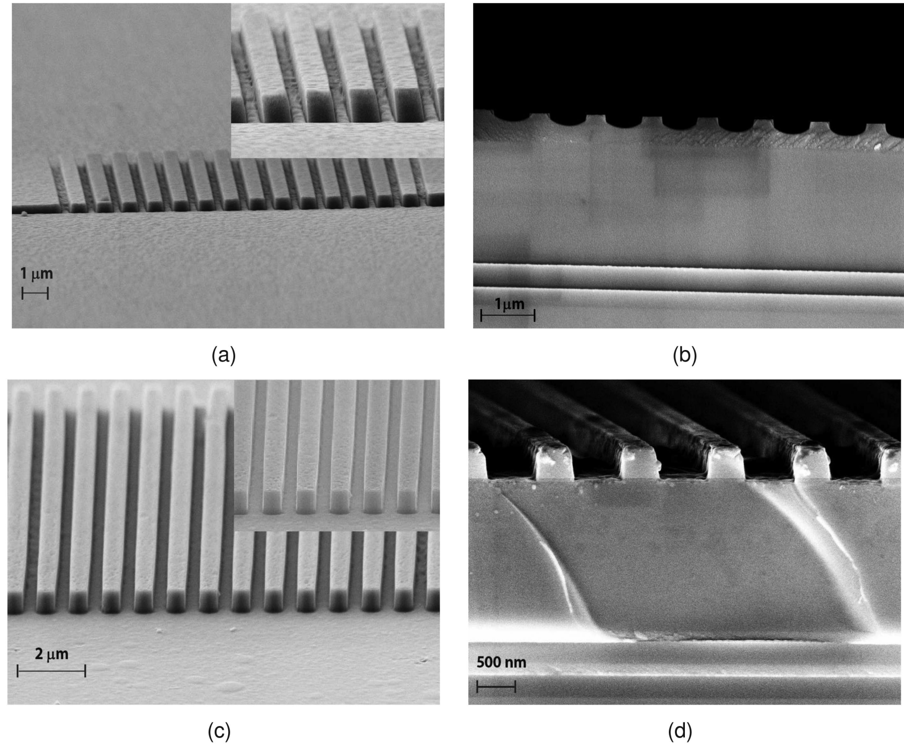

(a) (b) (c) (d)

Fig. 11. (a) Top view SEM of the fabricated devices for partially etched 500 nm SiN gratings and (b) its side view cross section with the bottom DBR stack. (c) Top view of fully etched 400 nm SiN gratings and (d) its side view with bottom DBR stack, both prior to top layer SiO_2 deposition.

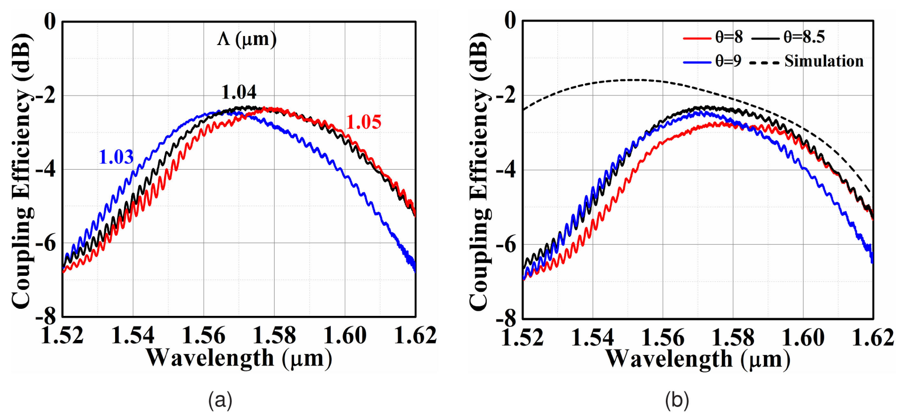

(a) (b)

Fig. 12. Measured coupling efficiency from patch 500 nm SiN waveguide test structure. Effect of (a) period at 8.5° fiber inclination angle θ (b) shows θ dependence at 1.04 μm period grating period with the dashed line corresponding to simulated curve at 1.04 μm period, 8.5° θ and 55% duty cycle.

the grating period, that agrees with the simulated value of 1 nm/nm. Fig. 12(b) shows the angle dependence of the peak measured period and its corresponding simulated spectrum. Fig. 13 shows the coupling efficiencies of the 400 nm thick SiN/SiO_2 grating devices. A maximum coupling efficiency of −2.58 dB per coupler is measured at 1576 nm with a 1 dB bandwidth of 52 nm. The maximum efficiency was achieved with a period of 1.12 μm, 60% duty-cycle and 8° inclination angle. A 20 nm variation in the grating period has only a marginal change in the coupling efficiency

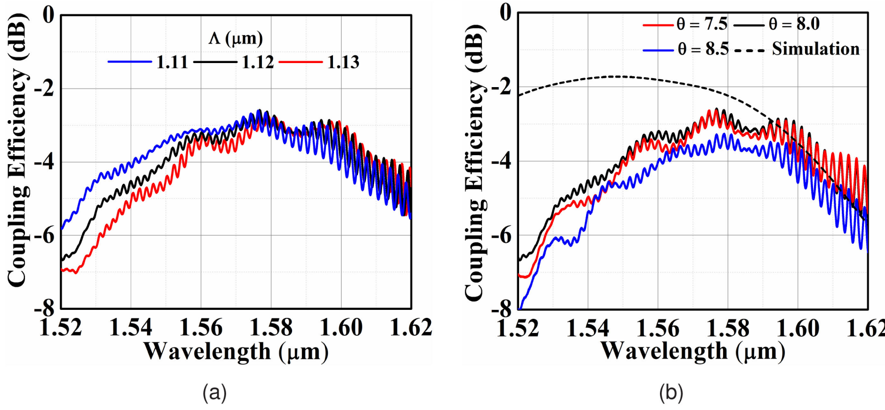

Fig. 13. Similarly, measured coupling efficiency from 400 nm *SiN* patch waveguide test structure. Effect of (a) period at 8° θ and (b) shows θ dependence at 1.12 μm period. The dashed line shows the simulated coupling at 8° with 1.12 μm period and 60% duty cycle.

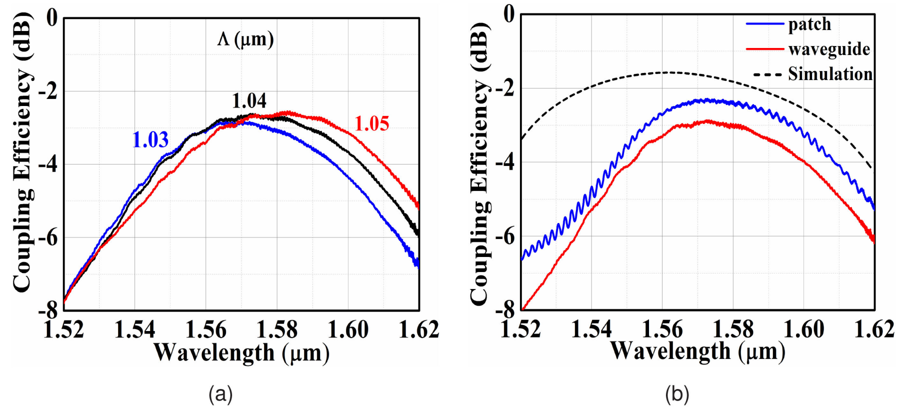

Fig. 14. Measured coupling efficiency to a 500 nm thick rib waveguide. (a) shows spectral shift with varying period at 55% duty cycle and 8.5° θ. (b) depicts the coupling comparison between a patch, rib waveguide and the simulated coupling (dashed line) at 1.05 μm period, 8.5° θ and 260 nm etch depth.

$\pm$0.13 dB. It is noticed that the peak coupling angle as well as wavelength and bandwidths for both platforms differs from that of simulated results. This may be attributed to a less than optimum duty cycle and etch depth (as in case of 500 nm *SiN*/air design) for the fabricated devices. In the case of patch waveguide test devices for both platforms, we observe periodic ripples which can be attributed to Fabry-Perot cavity effect stemming due to its short length. We observe a ripple period of 2 nm that corresponds to a cavity length of 300 nm in *SiN* which also confirms the origin of the ripples. Fig. 14(a) depicts the measured coupling efficiency for different periods between a fiber and a rib waveguide on the 500 nm *SiN*/air grating platform (with dimensions, illustrated in Fig. 9(b)). We measure a peak efficiency of -2.84 dB per coupler. A comparison of measured efficiencies of the patch grating, rib waveguide and the simulated spectrum is plotted in Fig. 14(b). The patch grating efficiency is $\approx$0.55 dB higher than the patch waveguide test device. We attribute the excess loss to a less than optimal 300 μm long waveguide taper. The taper loss can be reduced by using either longer adiabatic tapers [11], focusing gratings [12] or compact tapers [39]. Since the test structure has smooth transition due to adiabatic tapering, we do not observe any ripples in the measured spectrum. Additional propagation loss due to scattering could be reduced by optimizing the patterning process [24]. The grating coupler efficiency could be further increased by using apodized grating to achieve better mode matching between the grating and fiber fields. It may be

TABLE 1
Comparison of Different Grating Couplers Demonstrated on Stand-Alone SiN Platforms in Visible and NIR Regions

SiN Coupler	Max. CE (dB)	1 dB Band-width (nm)	λ_{max} (μm)	t_{SiN} (nm)	Upper Cladding	SiN type	Bottom reflector	Grating type
Ref. [9]	-4.2	67	1.57	400	SiO_2	LPCVD	N	Uniform
Ref. [11]	-2.5	53	1.49	400	SiO_2	LPCVD	Y	Uniform
Ref. [12]	-3.7	54	1.555	700	air	LPCVD	N	Uniform
Ref. [14]	-6.5	55	1.541	360	SiO_2	LPCVD	N	Uniform, TM grating
Ref. [13]	-1.5	60 (3 dB)	1.555	600	air	LPCVD	N	Non-uniform, staircase
Ref. [32]	-2.56	46.9	1.54	220	SiO_2	PECVD	N	Non-uniform, bi-layer
Ref. [40]	-2.2	-	1.31	300	SiO_2	LPCVD	N	Uniform
Ref. [41]	-5.7	26	0.91	220	SiO_2	PECVD	N	Uniform
Ref. [22]	-2.29	-	0.66	100	SiO_2	PECVD	Y	Uniform
This work	-2.29	49	1.573	500	air	PECVD	Y	Uniform
This work	-2.58	52	1.576	400	SiO_2	PECVD	Y	Uniform

mentioned that, though the 500 nm partially etched SiN/air grating would have a better coupling performance on account of improved grating strength, the former may not always be feasible in an integrated platform. However such designs can be considered for sensing applications or nonlinear photonics where surrounding cladding can critically impact waveguide dispersion. In Table 1, we compare the demonstrated coupler performance, among different SiN platforms reported so far in literature.

5. Conclusion

In summary, we have designed, fabricated and experimentally demonstrated grating couplers on two distinct platforms of PECVD SiN. We have presented a detailed design, analysis and fabrication of grating couplers having high directionality. Using bottom Bragg reflectors, we demonstrate a measured peak coupling efficiency of -2.29 dB and -2.58 dB in 500 nm thick SiN/air and 400 nm thick SiN/SiO_2 gratings respectively. To the best of our knowledge, the demonstrated efficiencies are the highest for 500 nm thick SiN and among the best for 400 nm thick SiN films when compared to couplers on LPCVD deposited films. Moreover, the minimum feature dimensions are compatible with Deep-UV lithography patterning technique. The low temperature and high-efficiency grating coupler demonstration shows a promising route for integration of SiN circuits on a variety of substrates.

References

[1] S. Romero-García, F. Merget, F. Zhong, H. Finkelstein, and J. Witzens, “Silicon nitride CMOS-compatible platform for integrated photonics applications at visible wavelengths,” *Opt. Express*, vol. 21, no. 12, pp. 14036–14046, 2013. [Online]. Available: http://www.opticsexpress.org/abstract.cfm?URI=oe-21-12-14036
[2] L. Hoffman *et al.*, “Low loss CMOS-compatible PECVD silicon nitride waveguides and grating couplers for blue light optogenetic applications,” *IEEE Photon. J.*, vol. 8, no. 5, Oct. 2016, Art. no. 2701211.
[3] A. Rahim *et al.*, “Expanding the silicon photonics portfolio with silicon nitride photonic integrated circuits,” *J. Lightw. Technol.*, vol. 35, no. 4, pp. 639–649, Feb. 2017.
[4] R. Baets *et al.*, “Silicon Photonics: Silicon nitride versus silicon-on-insulator,” in *Proc. Opt. Fiber Commun. Conf.*, 2016, Paper Th3J.1. [Online]. Available: https://www.osapublishing.org/abstract.cfm?URI=OFC-2016-Th3J.1

[5] P. Muoz *et al.*, “Foundry developments toward silicon nitride photonics from visible to the mid-infrared,” *IEEE J. Sel. Topics Quantum Electron.*, vol. 25, no. 5, Sep./Oct. 2019, Art. no. 8200513.
[6] A. Fülöp, C. J. Krückel, D. Castelló-Lurbe, E. Silvestre, and V. Torres-Company, “Triply resonant coherent four-wave mixing in silicon nitride microresonators,” *Opt. Lett.*, vol. 40, no. 17, pp. 4006–4009, 2015. [Online]. Available: http://ol.osa.org/abstract.cfm?URI=ol-40-17-4006
[7] S. Kim *et al.*, “Dispersion engineering and frequency comb generation in thin silicon nitride concentric microresonators,” *Nature Commun.*, vol. 8, no. 1, 2017, Art. no. 372. [Online]. Available: http://www.nature.com/articles/s41467-017-00491-x
[8] J. S. Levy, A. Gondarenko, M. A. Foster, A. C. Turner-Foster, A. L. Gaeta, and M. Lipson, “CMOS-compatible multiple-wavelength oscillator for on-chip optical interconnects,” *Nature Photon.*, vol. 4, no. 1, pp. 37–40, 2010. [Online]. Available: http://www.nature.com/doifinder/10.1038/nphoton.2009.259
[9] C. R. Doerr, L. Chen, Y. K. Chen, and L. L. Buhl, “Wide bandwidth silicon nitride grating coupler,” *IEEE Photon. Technol. Lett.*, vol. 22, no. 19, pp. 1461–1463, Oct. 2010.
[10] H. Zhang, C. Li, X. Tu, X. Luo, M. Yu, and P. G.-Q. Lo, “High efficiency silicon nitride grating coupler,” *Appl. Phys. A*, vol. 115, no. 1, pp. 79–82, 2014. [Online]. Available: http://link.springer.com/10.1007/s00339-013-7954-2
[11] H. Zhang *et al.*, “Efficient silicon nitride grating coupler with distributed Bragg reflectors,” *Opt. Express*, vol. 22, no. 18, pp. 21800–21805, Sep. 2014. [Online]. Available: http://www.opticsexpress.org/abstract.cfm?URI=oe-22-18-21800
[12] X. Zhao *et al.*, “Compact grating coupler for 700-nm silicon nitride strip waveguides,” *J. Lightw. Technol.*, vol. 34, no. 4, pp. 1322–1327, Feb. 2016. [Online]. Available: https://ieeexplore.ieee.org/document/7360098
[13] Y. Chen *et al.*, “Experimental demonstration of an apodized-imaging chip-fiber grating coupler for Si_3N_4 waveguides,” *Opt. Lett.*, vol. 42, no. 18, pp. 3566–3569, 2017. [Online]. Available: http://ol.osa.org/abstract.cfm?URI=ol-42-18-3566
[14] G. Dabos *et al.*, “TM grating coupler on low-loss LPCVD based Si_3N_4 waveguide platform,” *Opt. Commun.*, vol. 405, pp. 35–38, 2017. [Online]. Available: http://www.sciencedirect.com/science/article/pii/S0030401817306752
[15] N. Daldosso *et al.*, “Fabrication and optical characterization of thin two-dimensional Si_3N_4 waveguides,” *Mater. Sci. Semicond. Process.*, vol. 7, no. 4–6, pp. 453–458, 2004.
[16] K. Foubert *et al.*, “Near-field modal microscopy of subwavelength light confinement in multimode silicon slot waveguides,” *Appl. Phys. Lett.*, vol. 93, no. 25, 2008, Art. no. 251103.
[17] K. Luke, A. Dutt, C. B. Poitras, and M. Lipson, “Overcoming Si_3N_4 film stress limitations for high quality factor ring resonators,” *Opt. Express*, vol. 21, no. 19, pp. 22829–22833, Sep. 2013. [Online]. Available: http://www.opticsexpress.org/abstract.cfm?URI=oe-21-19-22829
[18] A. Gondarenko, J. S. Levy, and M. Lipson, “High confinement micron-scale silicon nitride high Q ring resonator,” *Opt. Express*, vol. 17, no. 14, pp. 11366–11370, Jul. 2009. [Online]. Available: http://www.opticsexpress.org/abstract.cfm?URI=oe-17-14-11366
[19] M. H. P. Pfeiffer *et al.*, “Photonic Damascene process for integrated high-Q microresonator based nonlinear photonics,” *Optica*, vol. 3, no. 1, pp. 20–25, Jan. 2016. [Online]. Available: http://www.osapublishing.org/optica/abstract.cfm?URI=optica-3-1-20
[20] K. N. Andersen, W. E. Svendsen, T. Stimpel-Lindner, T. Sulima, and H. Baumgärtner, “Annealing and deposition effects of the chemical composition of silicon-rich nitride,” *Appl. Surface Sci.*, vol. 243, no. 1, pp. 401–408, 2005. [Online]. Available: http://www.sciencedirect.com/science/article/pii/S0169433204014473
[21] C. J. Krückel, A. Fülöp, T. Klintberg, J. Bengtsson, P. A. Andrekson, and V. Torres-Company, “Linear and nonlinear characterization of low-stress high-confinement silicon-rich nitride waveguides,” *Opt. Express*, vol. 23, no. 20, pp. 25827–25837, 2015. [Online]. Available: https://www.osapublishing.org/abstract.cfm?URI=oe-23-20-25827
[22] S. Romero-García, F. Merget, F. Zhong, H. Finkelstein, and J. Witzens, “Visible wavelength silicon nitride focusing grating coupler with AlCu/TiN reflector,” *Opt. Lett.*, vol. 38, no. 14, pp. 2521–2523, Jul. 2013. [Online]. Available: http://ol.osa.org/abstract.cfm?URI=ol-38-14-2521
[23] Y. H. D. Lee and M. Lipson, “Back-end deposited silicon photonics for monolithic integration on CMOS,” *IEEE J. Sel. Top. Quantum Electron.*, vol. 19, no. 2, Mar. 2013, Art. no. 8200207.
[24] J. M. Shainline *et al.*, “Room-temperature-deposited dielectrics and superconductors for integrated photonics,” *Opt. Express*, vol. 25, no. 9, pp. 10322–10334, 2017. [Online]. Available: https://www.osapublishing.org/abstract.cfm?URI=oe-25-9-10322
[25] T. Wang *et al.*, “Supercontinuum generation in bandgap engineered, back-end CMOS compatible silicon rich nitride waveguides,” *Laser Photon. Rev.*, vol. 9, no. 5, pp. 498–506, 2015.
[26] K. J. A. Ooi *et al.*, “Pushing the limits of CMOS optical parametric amplifiers with USRN:Si7N3 above the two-photon absorption edge,” *Nature Commun.*, vol. 8, Jan. 2017, Art. no. 13878. [Online]. Available: https://doi.org/10.1038/ncomms13878 http://10.0.4.14/ncomms13878 https://www.nature.com/articles/ncomms13878#supplementary-information
[27] C. Lacava *et al.*, “Si-rich silicon nitride for nonlinear signal processing applications,” *Sci. Rep.*, vol. 7, no. 1, 2017, Art. no. 22. [Online]. Available: http://www.nature.com/articles/s41598-017-00062-6
[28] K. Ikeda, R. E. Saperstein, N. Alic, and Y. Fainman, “Thermal and Kerr nonlinear properties of plasma-deposited silicon nitride/ silicon dioxide waveguides,” *Opt. Express*, vol. 16, no. 17, pp. 12987–12994, 2008. [Online]. Available: https://www.osapublishing.org/oe/abstract.cfm?uri=oe-16-17-12987
[29] L. Wang, W. Xie, D. V. Thourhout, Y. Zhang, H. Yu, and S. Wang, “Nonlinear silicon nitride waveguides based on a PECVD deposition platform,” *Opt. Express*, vol. 26, no. 8, pp. 9645–9654, Apr. 2018. [Online]. Available: http://www.opticsexpress.org/abstract.cfm?URI=oe-26-8-9645
[30] T. D. Bucio *et al.*, “Material and optical properties of low-temperature NH_3-free PECVD SiN x layers for photonic applications,” *J. Phys. D. Appl. Phys.*, vol. 50, no. 2, 2017, Art. no. 25106. [Online]. Available: http://stacks.iop.org/0022-3727/50/i=2/a=025106
[31] Z. Shao *et al.*, “Ultra-low temperature silicon nitride photonic integration platform,” *Opt. Express*, vol. 24, no. 3, pp. 1865–1872, 2016. [Online]. Available: https://www.osapublishing.org/abstract.cfm?URI=oe-24-3-1865

[32] E. W. Ong, N. M. Fahrenkopf, and D. D. Coolbaugh, “SiNx bilayer grating coupler for photonic systems,” *OSA Contin.*, vol. 1, no. 1, pp. 13–25, Sep. 2018. [Online]. Available: http://www.osapublishing.org/osac/abstract.cfm?URI=osac-1-1-13

[33] S. Nambiar, A. Kumar, K. Rakshitha, P. Ranganath, and S. K. Selvaraja, “High-efficiency SiN grating fiber-chip coupler with bottom reflector,” in *Proc. Eur. Conf. Integr. Opt.*, Jun. 2018, pp. 1–3.

[34] Y. Ding, C. Peucheret, H. Ou, and K. Yvind, “Fully etched apodized grating coupler on the SOI platform with −0.58 dB coupling efficiency,” *Opt. Lett.*, vol. 39, no. 18, pp. 5348–5350, Sep. 2014. [Online]. Available: http://ol.osa.org/abstract.cfm?URI=ol-39-18-5348

[35] C. Kopp, E. Augendre, R. Orobtchouk, O. Lemonnier, and J. M. Fedeli, “Enhanced fiber grating coupler integrated by wafer-to-wafer bonding,” *J. Lightw. Technol.*, vol. 29, no. 12, pp. 1847–1851, Jun. 2011.

[36] W. S. Zaoui *et al.*, “Bridging the gap between optical fibers and silicon photonic integrated circuits,” *Opt. Express*, vol. 22, no. 2, pp. 1277–1286, 2014. [Online]. Available: https://www.osapublishing.org/oe/abstract.cfm?uri=oe-22-2-1277

[37] S. K. Selvaraja *et al.*, “Highly efficient grating coupler between optical fiber and silicon photonic circuit,” in *Proc. Conf. Lasers Electro Opt. Conf. Quantum Electron. Laser Sci. Conf.*, Jun. 2009, pp. 1–2.

[38] D. Taillaert, P. Bienstman, and R. Baets, “Compact efficient broadband grating coupler for silicon-on-insulator waveguides,” *Opt. Lett.*, vol. 29, no. 23, pp. 2749–2751, Dec. 2004. [Online]. Available: http://ol.osa.org/abstract.cfm?URI=ol-29-23-2749

[39] P. Sethi, R. Kallega, A. Haldar, and S. K. Selvaraja, “Compact broadband low-loss taper for coupling to a silicon nitride photonic wire,” *Opt. Lett.*, vol. 43, no. 14, pp. 3433–3436, Jul. 2018. [Online]. Available: http://ol.osa.org/abstract.cfm?URI=ol-43-14-3433

[40] G. Maire *et al.*, “High efficiency silicon nitride surface grating couplers,” *Opt. Express*, vol. 16, no. 1, pp. 328–333, Jan. 2008. [Online]. Available: http://www.opticsexpress.org/abstract.cfm?URI=oe-16-1-328

[41] A. Z. Subramanian, S. Selvaraja, P. Verheyen, A. Dhakal, K. Komorowska, and R. Baets, “Near-infrared grating couplers for silicon nitride photonic wires,” *IEEE Photon. Technol. Lett.*, vol. 24, no. 19, pp. 1700–1703, Oct. 2012.